

Debiasing Machine Learning Predictions for Causal Inference Without Additional Ground Truth Data: “One Map, Many Trials” in Satellite-Driven Poverty Analysis

Markus Pettersson, *Chalmers*

Connor T. Jerzak, *UT Austin* Adel Daoud, *Chalmers & Linköping University*

Correspondence: markus.pettersson@chalmers.se

August 5, 2025

Abstract

Machine learning models trained on Earth observation data, such as satellite imagery, have demonstrated significant promise in predicting household-level wealth indices, enabling the creation of high-resolution wealth maps that can be leveraged across multiple causal trials while addressing chronic data scarcity in global development research. However, because standard training objectives prioritize overall predictive accuracy, these predictions inherently suffer from shrinkage toward the mean, leading to attenuated estimates of causal treatment effects and limiting their utility in policy evaluations. Existing debiasing methods, such as Prediction-Powered Inference (PPI), can handle this attenuation bias but require additional fresh ground-truth data at the downstream stage of causal inference, which restricts their applicability in data-scarce environments. In this paper, we introduce and evaluate two correction methods—linear calibration correction and Tweedie’s correction—that substantially reduce prediction bias without relying on newly collected labeled data. Linear calibration (LCC) corrects bias through a straightforward linear transformation derived from held-out calibration data, whereas Tweedie’s correction leverages empirical Bayes principles to directly address shrinkage-induced biases by exploiting score functions derived from evaluating the model’s learning patterns. Through analytical exercises and experiments using Demographic and Health Survey (DHS) data, we demonstrate that both proposed methods meet or outperform existing approaches that either require (a) adjustments to training pipelines or (b) additional labeled data, achieving significant reductions in attenuation bias in data-scarce environments. These approaches may represent a promising avenue for improving the reliability of causal inference when direct outcome measures are limited or unavailable, enabling a “one map, many trials” paradigm where a single upstream data creation team produces predictions usable by many downstream teams across diverse ML pipelines.

Introduction

Machine learning (ML) models trained on Earth observation (EO) data have recently demonstrated impressive performance in predicting household-level wealth indices, such as the International Wealth Index (IWI), with reported R^2 values approaching 0.80 [Pettersson et al., 2023, Jean et al., 2016, Daoud et al., 2023, Chi et al., 2022]. These EO-ML models offer a much-needed solution to longstanding data scarcity issues in global development, enabling researchers to generate high-resolution, retrospective “wealth maps” in data-poor regions. But while these predictions are promising in the EO-ML upstream task, a key question remains [Jerzak et al., 2023a,b]: the value of EO-ML-derived data hinges on whether domain researchers, in the downstream phase, can use these data to estimate causal effects for their specific application area down-

stream of the research process, from evaluating applied environmental to social science questions Daoud and Dubhashi [2023].

However, even under ideal conditions, the predictions of EO-ML models tend to have a smaller variance than the target values, leading to attenuated treatment effects and, thus, potentially misleading conclusions [Berglund, 2012].

Recent research has developed methods that can debias the upstream EO-ML model, but they require either fresh data in the downstream Olofsson et al. [2013], Egami et al. [2023], Lu et al. [2024] or changing the way the model is trained Ratledge et al. [2022]. For example, relying on such fresh data, Angelopoulos et al. [2023] proposes Prediction-Powered Inference (PPI), a method that corrects any ML model for downstream inference. Similarly, Egami et al. [2023] achieves the same goal but with better sample efficiency de Pieuchon et al. [2025], but it also requires knowing the probability of observing a sample point. While these methods offer a path to integrate upstream and downstream analyses, their success depends on the sometimes availability of newly collected treatment-predictor-outcome tuples in the downstream causal step or knowledge of the data labeling process [Egami et al., 2023]. Often, such data are prohibitively costly or unethical to collect.

Ratledge et al. [2022] addresses the challenge of attenuation bias and the unavailability of data in the downstream by adjusting the model’s loss function instead. During training, they penalize quintile-level discrepancies between observed and predicted means, encouraging predictions to match the true outcome distribution more closely across its support. Although their solutions do not need additional downstream data, they require modifying the training pipeline, which is likely computationally expensive.

Thus, to enable broader applicability of ML models, the upstream team needs to create a data product that is agnostic to downstream use, requires no downstream-fresh data, produces unbiased causal estimates (due to attenuation), and is computationally efficient Daoud and Dubhashi [2023].

We address this gap by proposing Tweedie’s correction, a novel method that reduces prediction bias without requiring fresh labeled data. We evaluate this approach against four others: linear calibration correction, Prediction-Powered Inference (PPI), the loss adjustment approach of Ratledge et al. [2022], and naive uncorrected predictions. The Tweedie’s correction paves the way for the same wealth map to be reused across multiple trials without needing to refit a model for each trial. This also removes the requirement for interaction between the upstream machine-learning team creating the data product and any other domain-knowledge team in the downstream phase. Hence the concept: *one map, many trials*. We derive analytical proofs and demonstrate the empirical performance of all methods in both simulations and real-world applications, using data from the African Demographic and Health Survey (DHS).

1 Problem Setup & Related Work

Statistical predictions can systematically shrink estimates toward the central modes of the training distribution [Ting, 2024a]. This phenomenon is rooted in optimal error-minimization estimation (cf. Stein’s paradox), where a model “hedges” predictions in regions of greater uncertainty. When facing noise or limited training data, the optimal strategy, in terms of minimizing residuals, is to pull predictions toward denser regions of the training data. For instance, consider an image that appears with an IWI of 80, but the model has observed this outcome only once, compared to thousands of observations with an IWI of around 70. A perfect prediction would be 80 for this data point, but the model will pull this data point’s prediction towards 70 instead to hedge against the risk of overcommitting to a rare value.

When such biased predictions replace true outcomes in downstream causal analyses, the resulting regression-to-the-mean induces attenuation bias, reducing observed treatment group differences even under randomization [Shu and Yi, 2019]. The difference in mean predicted outcomes between treated and control units shrinks both group means toward the global average, thereby attenuating the estimated effect.

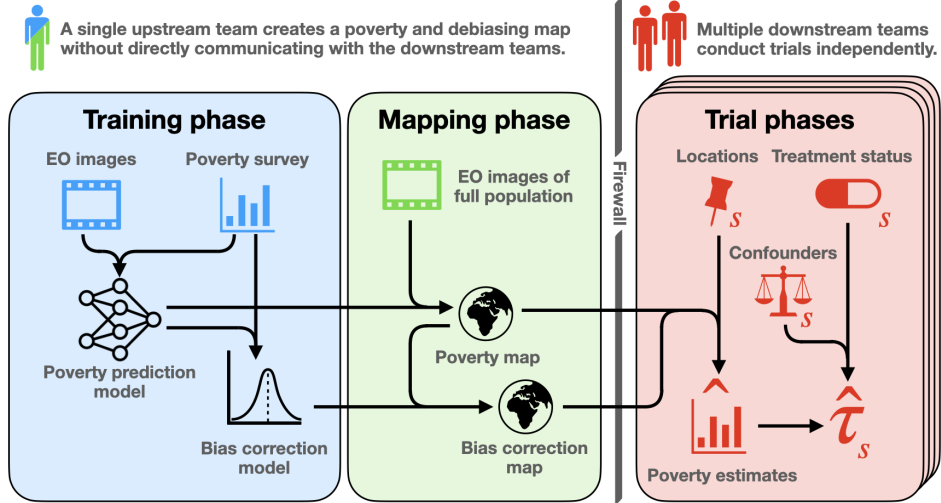


Figure 1: Illustrating the proposed debiasing pipeline for causal inference using machine learning predictions from satellite imagery, without requiring fresh ground-truth data.

Regression-to-the-mean bias is particularly acute in upstream tasks with scarce ground truth (due to finite samples) or in high-dimensional input data (due to the curse of dimensionality), forcing greater reliance on error-prone predictions—something especially pertinent in development economics, political science, and global health contexts—where household data is often expensive or unavailable—to increasingly substitute upstream predictions [Kino et al., 2021, Kakooei et al., 2024, Daoud and Johansson, 2024]. Moreover, high out-of-sample R^2 does not eliminate this bias: models can achieve strong accuracy yet yield attenuated causal estimates [Ting, 2024b].

Existing remedies, such as PPI, which subtracts a rectifier estimated from fresh ground-truth pairs at the causal-inference stage [Angelopoulos et al., 2023], or loss-function adjustments that penalize quintile-level errors [Ratledge et al., 2022]. However, these approaches require that the upstream team adapts the data for downstream analysis, slowing or limiting altogether "one map, many trials" efforts.

To address these limitations, we propose a Tweedie-inspired method. This Tweedie method debiases the shrinkage effect in ML-predicted outcomes, enabling downstream researchers to accurately recover causal effects from the upstream data product. Our Tweedie approach treats the ML model as a black box: we assume access only to its out-of-sample predictions and do not rely on retraining or modifying the model. Under this setting, we demonstrate that shrinkage can be reversed, either by learning a global calibration correction from held-out labeled data or by estimating a local correction using ideas from Tweedie’s formula, initially described by Robbins and Tweedie in 1956. Both strategies aim to recover unbiased treatment effect estimates from biased predictions, without requiring fresh ground-truth labels at the time of intervention. We benchmark our Tweedie adaptation to existing methods, which are compared in Table A.III.1 based on their associated assumptions and data/training requirements. As previously mentioned, the only method we are unable to deploy in our setting is the DSL method, as the probability of DHS samples is a function of unknown aid disbursement strategies.

Setup

Our pipeline assumes access to two datasets. First, in the upstream, a labeled dataset with training points (with indices in $\mathcal{I}_{\text{Train}}$): $D_{\text{Train}} = \{(\mathbf{X}_i, Y_i) : i \in \mathcal{I}_{\text{Train}}\}$, where $\mathbf{X}_i \in \mathcal{X}$ denotes covariates (e.g., satellite imagery) and Y_i is the true, ground-truth outcome (e.g., IWI poverty level as from the DHS).

Next, in the downstream phase, we assume that different teams have assembled collections of trial

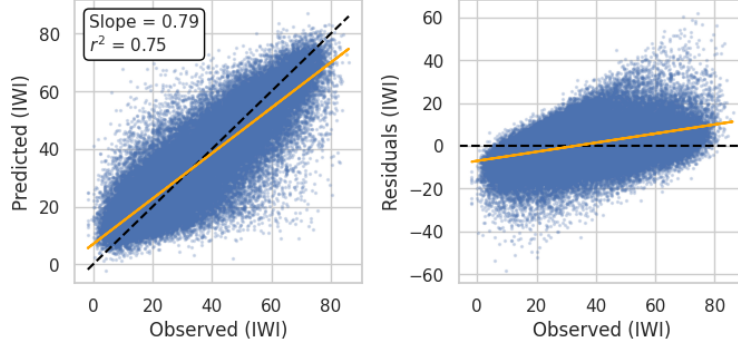


Figure 2: The left is a calibration plot of predicted versus true IWI values at held-out DHS clusters. The orange line shows that the predictions exhibit attenuation bias, resulting in overestimation of wealth for poorer locations and underestimation for wealthier ones. The dashed lines represent the ideal relationship. The right plot shows the residuals.

datasets indexed by s , corresponding to different randomized controlled trials, quasi-experiments, or geographic partitions, with a specific treatment (or action) of interest indexed by treatment setting: $D_{\text{Trial } s} = \{(\mathbf{X}_i, \hat{Y}_i, A_{is}) : i \in \mathcal{I}_{\text{Trial } s}, s \in \mathcal{S}\}$. The data product associated with Y_i is general (e.g., all-Africa), but investigators may want to use that data in multiple causal settings, s , each with a different treatment, $A_{is} \in \{0, 1\}$. The outcome Y_i is not directly observed for all i . Instead, inference will need to take place through the noisy variable, \hat{Y}_i . We henceforth remove dependence on s for simplicity.

A key idea henceforth is that the upstream team—the one machine-learning team—creates an *agnostic* dataset [Grimmer et al., 2022], meaning that this team’s data product should produce unbiased causal estimates for any number of applications (trials) for the variety of teams downstream. This implies that there is no communication between up and downstream teams—hence the firewall between the two phases.

2 Methodology

In this section, we present a suite of methods designed to debias treatment effect estimates that rely on ML-predicted outcomes. Our overarching goal is to mitigate regression-to-the-mean dynamics in the downstream analysis, improving estimates of causal effects or population-level statistics. We first more formally describe two existing solutions, *PPI* and the method of Ratledge et al. [2022], before introducing two no-new-data debiasing approaches—Linear Calibration Correction (LCC) and Tweedie’s Correction—that use held-out data (without requiring fresh labels in the causal step) to correct shrinkage bias.

PPI proposes a framework for valid statistical inference when a large set of unlabeled observations is paired with a predictive model’s outputs [Angelopoulos et al., 2023]. Concretely, letting θ^* be the target parameter (e.g., a population mean) and f denote the model that maps covariates \mathbf{X}_i to predicted outcomes $f(\mathbf{X}_i)$, PPI forms an estimator by adding a *rectifier* term—an adjustment for the average discrepancy between Y_i and $f(\mathbf{X}_i)$ observed in a smaller, labeled dataset. An estimate for θ^* is computed using an “imputed” version based on unlabeled data ($\{\mathbf{X}_i\}_{i=n+1}^N$), then corrected by subtracting the bias estimated on the labeled subset. For mean estimates, this adjustment is:

$$\hat{\theta}^{\text{PPI}} = \frac{1}{N-n} \sum_{i=n+1}^N f(\mathbf{X}_i) - \frac{1}{n} \sum_{i=1}^n (f(\mathbf{X}_i) - Y_i)$$

Because the rectifier is estimated on ground-truth pairs $\{\mathbf{X}_i, Y_i\}_{i=1}^n$, the procedure maintains valid coverage for θ^* in large samples, provided that the predictive model f is fixed (i.e., not retrained on the labeled data).

Unlike our approach, however, PPI crucially relies on gathering labeled observations in the downstream phase. Such labels come from high-quality surveys coordinated by USAID across the African continent and cost millions of US dollars to execute. Given the recent funding cuts to USAID, it is unlikely that new and fresh DHS data points will be collected. Hence, there is an acute need for unbiased data collection, which should be fully handled in the upstream phase. We will nonetheless include PPI correction in our analysis with the goal of showing *what would have happened to our estimates had fresh data actually been available downstream*.

Another approach to remedy attenuation bias is to adjust the loss function: Ratledge et al. [2022] propose a specialized upstream training procedure that directly penalizes quintile-level discrepancies between observed and predicted means, thereby encouraging \hat{Y}_i to match the true distribution of Y_i more closely across the support of the outcome distribution. Specifically, this approach modifies the model’s objective function, punishing a quintile having a higher MSE than the others:

$$\mathcal{L} = \text{MSE} + \lambda_b \hat{E}_b,$$

MSE is the mean squared error, $\lambda_r L_2$ is the L2 regularization term, and $\lambda_b \hat{E}_b$ is the quintile-specific bias loss, with $\hat{E}_b = \max_j (\hat{B}_j(\hat{f})^2)$ and $\hat{B}_j(\hat{f}) = \mathbb{E}[\hat{f}(\mathbf{X}_i) - Y_i \mid Y_i \in Q_j]$. By design, this approach reduces the likelihood that group-level estimates of causal effects are attenuated when \hat{Y}_i is used in downstream analyses. In contrast, our methods operate as post-hoc corrections on out-of-sample predictions from a black-box model, requiring no specialized retraining or customized loss function that might reduce overall predictive performance.

2.1 Linear Calibration Correction (LCC)

For LCC, we approximate the relationship between EO-ML predictions and ground-truth wealth on the held-out calibration set by a linear transformation:

$$\hat{Y}_i = kY_i + m,$$

where $0 < k \leq 1$ reflects shrinkage toward the mean and $m \in \mathbb{R}$ is the intercept, representing the mean fixed bias. This linearity might not always be empirically satisfied, but occurs regularly in our data (see, e.g., Figure A.III.3). When these predictions are used in place of true outcomes to estimate causal effects, this shrinkage attenuates estimated treatment effects.

Let $\tau = \mathbb{E}[Y_i \mid A_i = 1] - \mathbb{E}[Y_i \mid A_i = 0]$ denote the true Average Treatment Effect (ATE). Using \hat{Y}_i instead of Y_i for ATE estimation yields the bias shown in Proposition 2.1.

Proposition 2.1 (Attenuation bias under linear shrinkage) *Let Y_i be the true outcome and \hat{Y}_i an ML prediction obeying the linear calibration model:*

$$\hat{Y}_i = kY_i + m + e_i \quad (0 < k \leq 1, m \in \mathbb{R}),$$

with k and m constants, and e_i mean 0 noise. Let $A_i \in \{0, 1\}$ denote a binary treatment that is randomly assigned ($A_i \perp Y_i(a)$ for $a \in \mathcal{A}$). Define the true average treatment effect (ATE) $\tau := \mathbb{E}[Y_i(1)] - \mathbb{E}[Y_i(0)]$ and the estimate, $\hat{\tau}$, from difference in predicted expected outcome:

$$\hat{\tau} = \mathbb{E}[\hat{Y}_i \mid A_i = 1] - \mathbb{E}[\hat{Y}_i \mid A_i = 0].$$

Then $\mathbb{E}[\hat{\tau}] = k\tau$. That is, the ATE estimated on the predictions is multiplied by the shrinkage factor k and is therefore attenuated toward 0 whenever $k < 1$.

Proof sketch. Take expectations using linearity:

$$\begin{aligned}\hat{\tau} &= \mathbb{E}[\hat{Y}_i \mid A_i = 1] - \mathbb{E}[\hat{Y}_i \mid A_i = 0] \\ &= \mathbb{E}[kY_i + m \mid A_i = 1] - \mathbb{E}[kY_i + m \mid A_i = 0] = k\tau.\end{aligned}$$

Replacing observed with potential outcomes follows from randomization. The estimated ATE is biased downward by a factor of k .

Now, to adjust for this bias, we will estimate k and m on a held-out calibration set from the training data by regressing \hat{Y}_i on Y_i (i.e., fitting the linear model $\hat{Y}_i = \hat{k}Y_i + \hat{m} + e_i$, where e_i is the residual). We then invert this fitted relationship (solving for Y_i) to obtain a calibrated estimate, given by $\hat{Y}_i^L = \frac{\hat{Y}_i - \hat{m}}{\hat{k}}$, assuming residuals e_i with mean zero conditional on covariates, independent of treatment A_i . This calibrated estimator restores the scale of the outcome variable, yielding Proposition 2.2:

Proposition 2.2 (Consistency of the LCC-corrected estimator) *Under the conditions of Proposition 2.1, estimate (k, m) on an independent calibration sample and set:*

$$\hat{Y}_i^L := (\hat{Y}_i - \hat{m})/\hat{k}, \quad \hat{\tau}^L := \mathbb{E}[\hat{Y}_i^L \mid A_i = 1] - \mathbb{E}[\hat{Y}_i^L \mid A_i = 0].$$

If $(\hat{k}, \hat{m}) \xrightarrow{P} (k, m)$, and $k > 0$, then $\hat{\tau}^L \xrightarrow{P} \tau$; i.e., the linear calibration correction removes the attenuation bias.

Proof sketch. By Slutsky's theorem, since $(\hat{k}, \hat{m}) \xrightarrow{P} (k, m)$, it follows that:

$$\begin{aligned}\hat{Y}_i^L &= [[kY_i + m + e_i] - \hat{m}]/\hat{k} \\ &= (k/\hat{k})Y_i + (m - \hat{m})/\hat{k} + e_i/\hat{k} \rightarrow Y_i + e_i/k\end{aligned}$$

Hence,

$$\hat{\tau}^L \rightarrow \mathbb{E}[Y_i + e_i/k \mid A_i = 1] + \mathbb{E}[Y_i + e_i/k \mid A_i = 0] = \tau,$$

since $\mathbb{E}[e_i] = 0$ and under noise independence, $e_i \perp A_i$. A drawback is that we assume a linear model for the shrinkage; estimating \hat{m} and \hat{k} introduces another potential source of error.

2.2 Tweedie's Correction for Debiasing

To go beyond the linearity assumption in LCC, we now turn to Tweedie's formula, which allows us to correct shrinkage bias in machine learning predictions by estimating the true outcome as the prediction plus a term involving the derivative of the log-density of the predictions. We follow Efron [2011], who revised the classical results in the context of selection bias as an automatic bias-correction tool in an empirical Bayes framework. We leverage the same core insight here to adjust for regression-to-the-mean bias in satellite-imputed outcomes when analyzing causal effects.

Setup. We here treat the shrinkage mechanism probabilistically:

$$\begin{aligned}\hat{Y}_i &= kY_i + \varepsilon_i, \quad 0 < k \leq 1, \\ \varepsilon_i &\stackrel{\text{i.i.d.}}{\sim} \mathcal{N}(0, \sigma^2), \quad \varepsilon_i \perp (Y_i, A_i).\end{aligned}\tag{1}$$

The factor $k < 1$ pulls extreme Y_i values toward the center, lowering $\text{Var}(\hat{Y}_i)$ whenever σ^2 is not too large. Setting $k = 1$ recovers the additive-noise model sometimes used in empirical-Bayes texts [Efron, 2012], so (1) nests the classic case.

This noise model enables us to leverage Tweedie's formula to recover the posterior mean of the latent outcome, accounting for shrinkage without requiring linearity assumptions.

Posterior mean via a scaled Tweedie identity. Write $W_i := kY_i$. Then $\hat{Y}_i = W_i + \varepsilon_i$ with the same ε_i as above, and the *Tweedie score identity* (Efron 2011)¹ gives

$$\mathbb{E}[W_i \mid \hat{Y}_i = \hat{y}] = \hat{y} + \sigma^2 \partial_{\hat{y}} \log p_{\hat{Y}}(\hat{y}), \quad (2)$$

where $p_{\hat{Y}}$ is the marginal density of \hat{Y}_i ; Dividing by k recovers the latent outcome:

$$\mathbb{E}[Y_i \mid \hat{Y}_i = \hat{y}] = \frac{\hat{y} + \sigma^2 \partial_{\hat{y}} \log p_{\hat{Y}}(\hat{y})}{k}. \quad (3)$$

For causal estimation, the relevant posterior is conditional on treatment: $\mathbb{E}[Y_i \mid \hat{Y}_i = \hat{y}, A_i = a] = \frac{\hat{y} + \sigma^2 \partial_{\hat{y}} \log p_{\hat{Y} \mid A_i = a}(\hat{y})}{k}$, since the noise is independent of A_i but treatment shifts the distribution of Y_i .

By expressing the posterior mean of the scaled latent variable in terms of the score function, we obtain a convenient identity that underlies the Tweedie adjustment.

Debiased point estimate. Equation 3 motivates the Tweedie-adjusted outcome:

$$\tilde{Y}_i := \frac{\hat{Y}_i + \sigma^2 \partial_{\hat{y}} \log p_{\hat{Y} \mid A_i}(\hat{Y}_i)}{k}, \quad (4)$$

which depends solely on the prediction \hat{Y}_i , treatment A_i , and two nuisance parameters, k and σ^2 .

With this adjustment defined, we now establish its unbiasedness properties under the assumed model.

Proposition 2.3 (Unbiasedness) *Under model (1), $\mathbb{E}[\tilde{Y}_i \mid \hat{Y}_i, A_i] = \mathbb{E}[Y_i \mid \hat{Y}_i, A_i]$ and hence by iterated expectations, $\mathbb{E}[\tilde{Y}_i] = \mathbb{E}[Y_i]$.*

Proof Sketch. Take conditional expectations in (4) and apply the group-specific version of (3) and iterated expectations.

Having established the unbiasedness of the Tweedie-adjusted outcome both conditionally and unconditionally, we now leverage this property to demonstrate that a simple difference-in-means estimator based on these adjusted outcomes yields an unbiased estimate of the average treatment effect under random assignment.

Proposition 2.4 (Tweedie-corrected ATE) *Let $\hat{\tau}^T := \hat{\mathbb{E}}[\tilde{Y}_i \mid A_i = 1] - \hat{\mathbb{E}}[\tilde{Y}_i \mid A_i = 0]$, where $\hat{\mathbb{E}}$ denotes the sample mean. Under (1) and random assignment, $\mathbb{E}[\hat{\tau}^T] = \tau$.*

Proof Sketch. $\mathbb{E}[\tilde{Y}_i \mid A_i = a] = \mathbb{E}[Y_i \mid A_i = a]$ by Prop. 2.3; subtract.

Estimation

The parameters k and σ^2 come from a *held-out calibration set* $\mathcal{I}_{\text{cal}} \subset \mathcal{I}_{\text{Train}}$ upstream; scores are estimated downstream:

1. **Shrinkage factor k .** Regress \hat{Y}_i on Y_i : $\hat{Y}_i = \hat{k} Y_i + \hat{m} + \text{resid}$. We keep the slope \hat{k} (discarding the intercept, absorbed into Y_i).
2. **Noise variance σ^2 .** Use the residuals: $\hat{\sigma}^2 = |\mathcal{I}_{\text{cal}}|^{-1} \sum_{i \in \mathcal{I}_{\text{cal}}} (\hat{Y}_i - \hat{k} Y_i)^2$.

¹For any $Z = \theta + \varepsilon$ with $\varepsilon \sim \mathcal{N}(0, \sigma^2)$, $\mathbb{E}[\theta \mid Z = z] = z + \sigma^2 \partial_x \log p_Z(z)$.

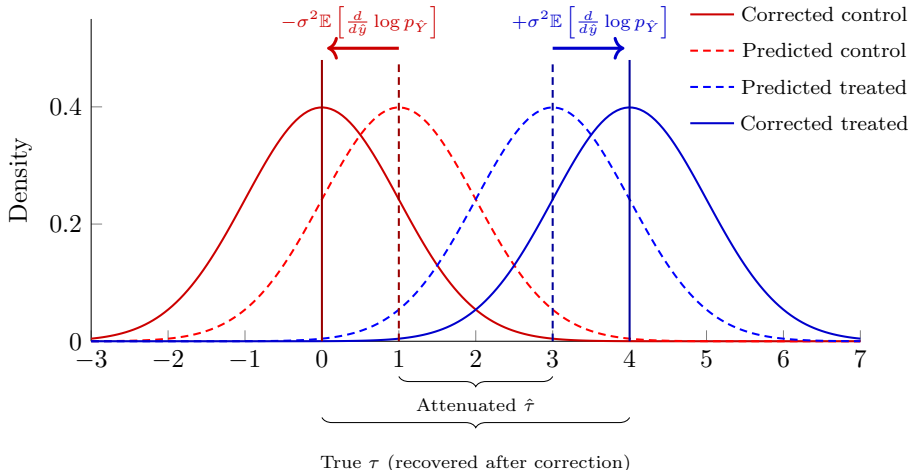


Figure 3: Illustration of Tweedie’s correction mechanism, showing how the posterior mean adjusts for shrinkage bias in predicted outcomes under Gaussian noise.

3. **Group-specific score functions** $\partial_{\hat{y}} \log p_{\hat{Y}|A_i=a}(\hat{y})$. Downstream, for each $a \in \{0, 1\}$, fit a smooth density $\hat{p}_{\hat{Y}|A_i=a}$ to $\{\hat{Y}_i : i \in \mathcal{I}_{\text{Trial}}, A_i = a\}$. Trim or regularize the derivative where $\hat{p}_{\hat{Y}|A_i=a}$ is small.

The operational formula passed downstream is in the end:

$$\hat{\tilde{Y}}_i = \frac{\hat{Y}_i + \hat{\sigma}^2 \partial_{\hat{y}} \log \hat{p}_{\hat{Y}|A_i}(\hat{Y}_i)}{\hat{k}}.$$

Relation to LCC. When the score term tends to zero (e.g., occurring when the variance on outcomes, Y_i , grows large), $\tilde{Y}_i = \hat{Y}_i/k$ —exactly an LCC correction. Tweedie’s adjustment, therefore, refines LCC with a *local, data-driven* addend that vanishes in regions where $p_{\hat{Y}|A_i}$ is flat and grows where shrinkage is most severe. For simplicity, we will, for all empirical Tweedie analyses henceforth, set $k = 1$ to isolate the performance contribution of the local, data-driven adjustment (versus that from the LCC-type correction).

3 Experiments with Simulated Data

Simulation Design. Our simulation study benchmarks all debiasing methods and monitors the upstream and downstream analyses while maintaining the firewall between them. The simulation uses a canonical directed acyclic graph (DAG), shown in Figure 4. It is *canonical* in the sense that the EO-ML literature tends to assume this structure [Sakamoto et al., 2025]. It illustrates the various research phases and their corresponding data availability.

In phase 0, the data-generation process (approximating *reality*) unfolds in the direction of the arrows. In the upstream phase, only the blue-nodes data are available, with finite samples of Y_i , to produce \hat{Y}_i for the entire population N . In the downstream, only red nodes are available: \hat{Y}_i is now available for N , jointly with C_i and A_{is} . They enable inference on the estimand τ_s . (We suppress the index s henceforth.) Appendix IV delineates our simulation further.

Simulation Results. We focus on two key objectives: minimizing error in the upstream task and minimizing causal bias in the downstream task. To assess error, we measure how closely the predicted values match

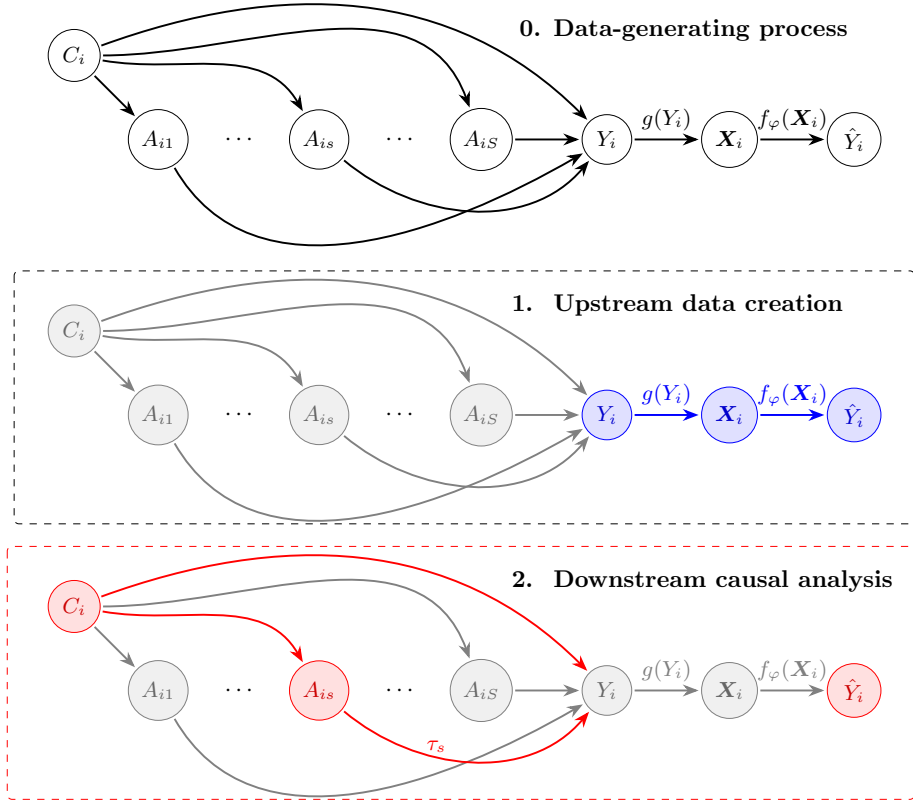


Figure 4: A panel illustrating data availability in the two phases.

0. Reality (data generation) shows the complete causal DAG.

1. **Upstream** phase: Y_i , X_i , and \hat{Y}_i are observed (blue).

2. **Downstream** phase: A_{is} , C_i , and \hat{Y}_i are available (red.)

the true values of τ , using Mean Absolute Error (MAE). A lower MAE indicates a more accurate estimation of the outcomes, and thus, a more accurate downstream ATE estimate. To assess bias, we examine the extent to which the upstream outcome prediction errors vary systematically when changing the magnitude of τ . This examination entails regressing the predicted $\hat{\tau}$ values on the true τ values and analyzing the calibration slope. If the estimates are unbiased, the slope should be close to one. Deviations from one indicate systematic over-/underestimation across the range of τ .

We can formally test deviations from 1 with an F -test: F -statistics from the above regression quantify the strength of the relationship between the predicted treatment effects and the true treatment effects. These F -statistic results (Table 1) indicate that Tweedie’s correction is the only method that yields ATE estimates for which we cannot reject the null hypothesis that these estimates are unbiased. Figure A.III.1 visualizes these slope results.

4 Experiments with Real Data

In this section, we conduct two types of downstream-real experiments. First, we will evaluate how well our debiasing methods succeed in descriptive tasks, especially those involving group aggregation. Second, we

Method	MAE	Slope	F -statistic	p -value
Tweedie’s	0.04	0.995	1.22	0.303
LCC	0.05	1.008	5.75	0.006
PPI (10%)	0.19	0.985	6.441	0.003
Ratledge	0.37	0.641	32.93	0.000
Naive	0.48	0.535	6420.43	0.000

Table 1: Simulation performance metrics. F -statistics and p -values are the statistical test for evaluating the null hypothesis that the slope value is 1. Failure to reject indicates that the slope estimate intervals contain the true ATE.

will apply our procedure to causal tasks. These two tasks cover the main use cases of our EO-ML-driven poverty data.

The full dataset consists of $n \approx 69,000$ geo-located survey clusters from the Demographic and Health Surveys (DHS) across 30 African countries (2009–2020), where each cluster comprises 20–30 households sampled via stratified two-stage design (primary sampling units selected with probability proportional to population size, followed by random household selection). We partitioned the data into five random folds for cross-validation (CV). For each run, four folds were used as upstream data (three for training, one for calibration): $D_{\text{Train}} = \{(\mathbf{X}_i, Y_i) : i \in \mathcal{I}_{\text{Train}}\}$. Downstream trial datasets $D_{\text{Trial } s}$ were drawn from the remaining, fifth fold and geo-referenced aid interventions, s , ensuring no overlap with training data.

Here, Y_i denotes the International Wealth Index (IWI), a continuous asset-based wealth score (0–100) aggregated at the cluster level to mitigate noise [Burke et al., 2021, Zhu et al., 2025]. The covariate array \mathbf{X}_i consists of Landsat satellite imagery (30m resolution, six multispectral bands) centered on each DHS cluster (6.72 km \times 6.72 km tiles), processed by taking the three-year median over cloud-free pixels leading up to the survey date.

Two models were fitted for each fold, one using MSE and one using the loss introduced by Ratledge et al. [2022]. The models shared the same ResNet-50 architecture and were initialized with weights pretrained on the SSL4EO-L dataset [Stewart et al., 2023]. For more details about model training, see Appendix II. The resulting MSE models all have an R^2 score between 0.74 and 0.76 on their hold-out fold, and an average slope of 0.79. Their combined predictions can be seen in Figure 2. The Ratledge models have a slope of 0.99, but at the cost of reduced R^2 scores between 0.67 and 0.70.

Estimating Region Means with Bias Adjustment. In our descriptive task, we estimate conditional means, averaging wealth by local second-level administrative region (ADM2), roughly corresponding to municipalities or counties. We group the clusters in the held-out downstream fold by ADM2 region and compare the mean observed IWI with the predicted IWI with and without the different methods of bias correction. These quantities are subject to the same shrinkage bias as causal estimates, and our framework applies equally well in this setting, enabling us to assess how effectively we correct biased group-level estimates.

Descriptive Results. As expected, the MSE of the naive model exhibits shrinkage behavior: it tends to overpredict the wealth of poorer regions and underpredict the wealth of richer regions. As shown in Figure 5, Tweedie’s correction accurately compensates for this, not only resulting in less biased estimates (regression slope of 0.83 to 0.90), but also decreases the MAE from 2.67 to 2.39. In fact, if we consider only regions with at least 100 clusters, the Tweedie-corrected estimates exhibit virtually no shrinkage bias, with a slope of 0.99. Appendix III delineates this analysis.

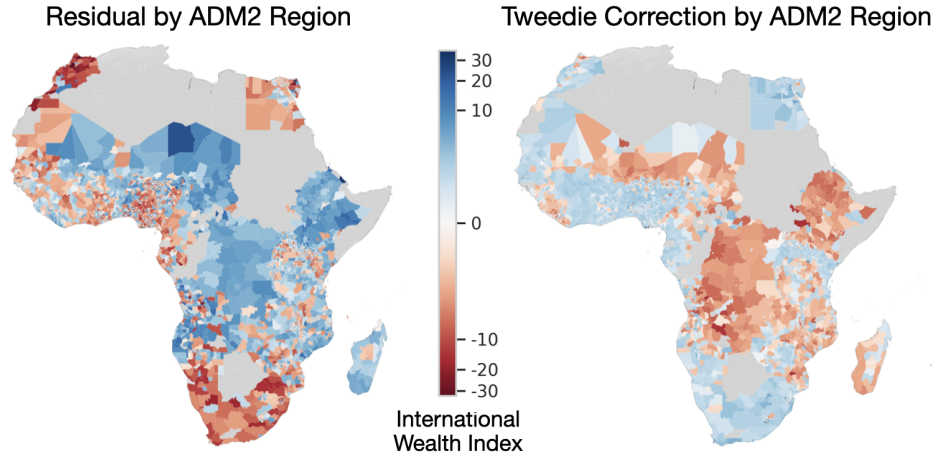


Figure 5: Mean residuals and Tweedie’s corrections for each ADM2 region in the dataset. regions that are overestimated in the left plot (blue) are shown to be correctly adjusted down in the right plot (red), and vice versa.

Empirical Analysis of Aid Interventions. To assess the practical utility of our correction methods in a setting where the true treatment effect is unknown, we construct an evaluation framework based on real-world development projects. Specifically, we leverage the same dataset of geo-referenced interventions funded by the World Bank and the Chinese government as was used in Malik et al. [2021], Conlin [2024]. Each project is tagged with an associated aid sector $s \in \mathcal{S}$ (e.g., *Health*, *Water Supply and Sanitation*, or *Women in Development*), which defines a downstream trial $D_{\text{Trial } s} = \{(\mathbf{X}_i, \hat{Y}_i, A_{is}) : i \in \mathcal{I}_{\text{Trial } s}\}$. Here, $A_{is} \in \{0, 1\}$ indicates exposure to a sector- s intervention at location i , \mathbf{X}_i are satellite features, and \hat{Y}_i are IWI predictions from the upstream-trained model. Figure A.III.2 depicts the spatial distribution of treatments across the continent.

Since the treatment effects of these interventions are unknown, we deem this analysis a test of external validity by comparing EO-ML predicted wealth values with observed ones. Our goal is to assess whether our bias-corrected predictions can reflect causal estimates similar to those from observed data.

To avoid label leakage and emulate real-world constraints, we perform a two-stage evaluation. We begin by randomly partitioning the available DHS survey data into two disjoint sets: an upstream set for training and calibrating the EO-ML model, and a downstream set used solely for evaluation. The model is trained on the upstream data, without any exposure to the intervention data or knowledge of future evaluation criteria. Shrinkage corrections (e.g., LCC or Tweedie’s correction) are also estimated on this upstream set.

We match project locations to the corresponding ADM2-level administrative regions, roughly equivalent to districts or municipalities. For a given funder-sector pair (e.g., Health projects funded by the World Bank), we identify all ADM2 regions containing at least one relevant intervention site. We then consider villages surveyed in the downstream DHS data within those regions, 3 to 8 years after the intervention, as the treated group. Villages in the same surveys, but outside the treated ADM2 regions, serve as controls.

For each funder-sector combination, we estimate the average treatment effect as the difference in mean outcomes between treated/control villages. We compute this using both observed IWI values and the model-predicted (and correction-adjusted) IWI values.

Causal Results. See Figure 6 for results. Each point is a causal study. While the x -axis shows what would have happened when using the label Y_i in these studies, the y -axis shows the corresponding causal effect using \hat{Y}_i with its corresponding adjustment approach. Orange lines check the correlation among these data. A score of one is perfect. The analysis shows that Tweedie’s correction (panel d) comes close to

this desiderata, with a correlation of 0.998; and it does so with the lowest MAE of 0.57. Had we used the naive predictions (panel *a*), the correlation would be 0.958 and the MAE would be 0.69. Assuming the PPI set up, with 10% fresh data available, we would have achieved a 0.981; and it does so with the lowest MAE of 0.73. The PPI performance is, however, a function of available data in the downstream, and panel *f* shows that with increasing fresh data, the PPI correction will outperform our Tweedie. But PPI is fresh-data hungry, and thus, this approach would come at a cost of deploying more costly surveys in Africa—costing downstream teams millions of USD de Pieuchon et al. [2025].

5 Discussion and Conclusion

Our experiments show that *post-hoc*, data-free corrections can eliminate the lion’s share of the shrinkage-induced attenuation that plagues causal analyses based on machine-learning predictions. In controlled simulations where the true ATE is known, Tweedie’s correction reduces mean-absolute error by an order of magnitude and, crucially, restores calibration: the fitted slope of $\hat{\tau}$ on τ is indistinguishable from one (Table 1, Figure A.III.1). The linear calibration correction also performs nearly as well despite its simplicity, suggesting that much of the bias arises from a first-order scaling distortion that can be identified on a small held-out calibration set. When applied to real DHS imagery, both corrections markedly narrow the gap between predicted and observed country-level means (Figure A.III.3), and in a quasi-experimental evaluation of large-scale aid projects, they bring estimated ATE into line with those obtained from ground-truth survey data (Figure 6).

For future research, we see three immediate research paths. First, formalize a theory of *adaptive corrections* that tunes the strength of Tweedie’s adjustment to local density estimates, thereby taming heteroskedasticity. Second, extend the methodology to multi-task settings where outcomes such as health, education, and nutrition are predicted jointly—an arena. Third, integrate causal discovery into the pipeline, allowing the system to learn when a variable is about to “debias” and find post-treatment leakage Daoud et al. [2022]. That would prevent the analyst from inadvertently resurrecting bias. It is important to note, however, that our methods specifically address attenuation bias arising from shrinkage and do not resolve all forms of bias in machine learning predictions; therefore, users should not regard the corrected predictions as fully unbiased. \square

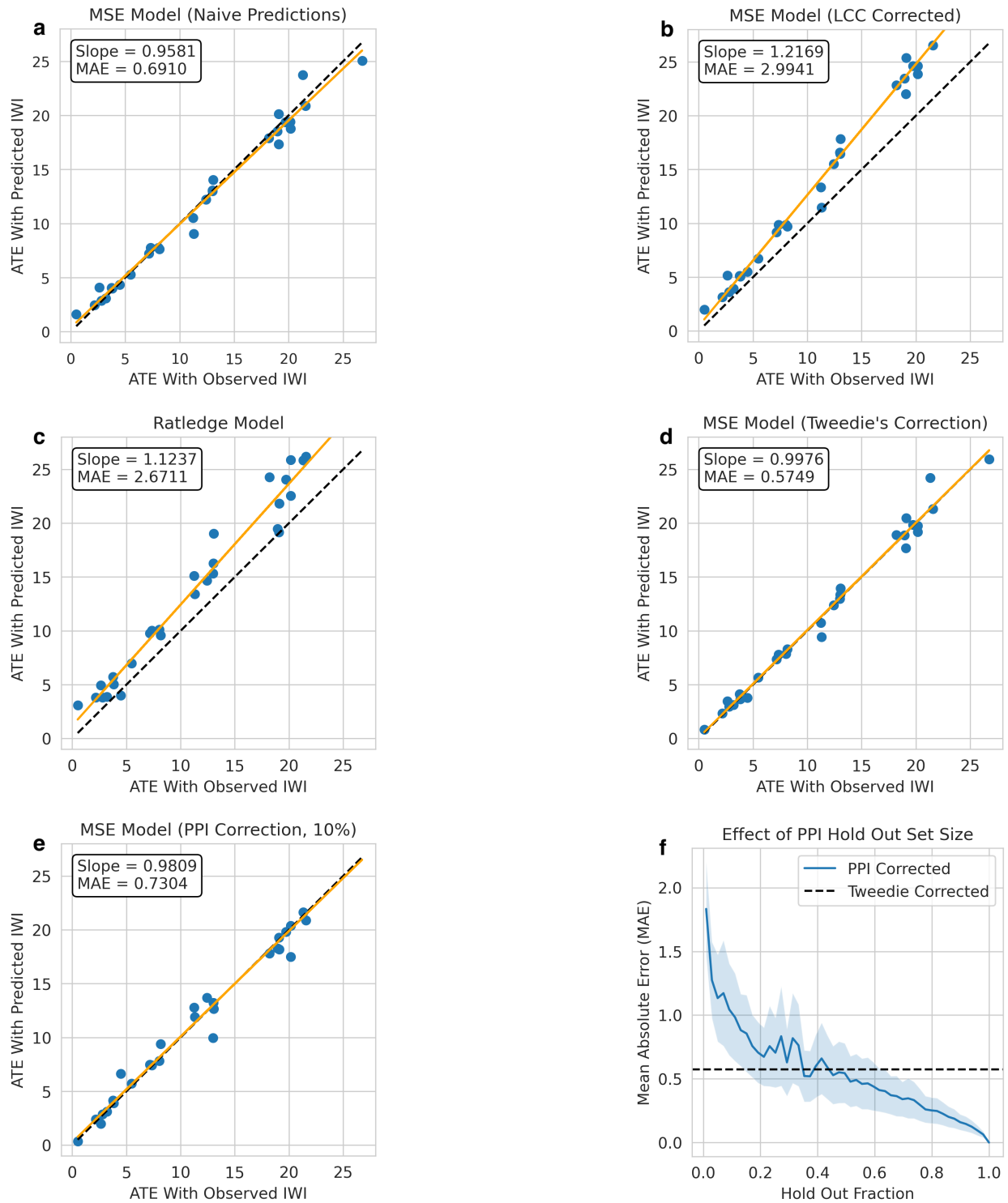


Figure 6: (a–e) Estimated treatment effects of aid interventions using unadjusted predictions, which display attenuation bias due to shrinkage. (f) PPI outperforms Tweedie’s correction in MAE bias reduction on larger hold-out sets, but requires many ground-truth labels.

References

- Anastasios N Angelopoulos, Stephen Bates, Clara Fannjiang, Michael I Jordan, and Tijana Zrnica. Prediction-powered inference. *Science*, 382(6671):669–674, 2023.
- Lars Berglund. Regression dilution bias: tools for correction methods and sample size calculation. *Upsala journal of medical sciences*, 117(3):279–283, 2012.
- Marshall Burke, Anne Driscoll, David B. Lobell, and Stefano Ermon. Using satellite imagery to understand and promote sustainable development. 371(6535):eabe8628, 2021. ISSN 0036-8075, 1095-9203. doi: 10.1126/science.abe8628. URL <https://www.sciencemag.org/lookup/doi/10.1126/science.abe8628>.
- Guanghua Chi, Han Fang, Sourav Chatterjee, and Joshua E Blumenstock. Microestimates of wealth for all low-and middle-income countries. *Proceedings of the National Academy of Sciences*, 119(3):e2113658119, 2022.
- Cindy Conlin. Using machine learning and daytime satellite imagery to estimate aid’s effect on wealth: Comparing china and world bank programs in africa. Master’s thesis, Linköping University, Department of Management and Engineering, The Institute for Analytical Sociology (IAS), Linköping, Sweden, June 2024. URL Available from: 2024-06-26. URN: urn:nbn:se:liu:diva-205256, ISRN: LIU-IEI-FIL-A-24/04656-SE.
- Adel Daoud and Devdatt Dubhashi. Statistical Modeling: The Three Cultures. 5(1), 2023. ISSN 2644-2353, 2688-8513. doi: 10.1162/99608f92.89f6fe66. URL <https://hdsr.mitpress.mit.edu/pub/uo4hjcx6/release/1>.
- Adel Daoud and Fredrik D. Johansson. The impact of austerity on children: Uncovering effect heterogeneity by political, economic, and family factors in low- and middle-income countries. 118:102973, 2024. ISSN 0049-089X. doi: 10.1016/j.ssresearch.2023.102973. URL <https://www.sciencedirect.com/science/article/pii/S0049089X2300128X>.
- Adel Daoud, Connor Jerzak, and Richard Johansson. Conceptualizing treatment leakage in text-based causal inference. In Marine Carpuat, Marie-Catherine de Marneffe, and Ivan Vladimir Meza Ruiz, editors, *Proceedings of the 2022 Conference of the North American Chapter of the Association for Computational Linguistics: Human Language Technologies*, pages 5638–5645, Seattle, United States, July 2022. Association for Computational Linguistics. doi: 10.18653/v1/2022.naacl-main.413. URL <https://aclanthology.org/2022.naacl-main.413/>.
- Adel Daoud, Felipe Jordán, Makkunda Sharma, Fredrik Johansson, Devdatt Dubhashi, Sourabh Paul, and Subhashis Banerjee. Using satellite images and deep learning to measure health and living standards in india. *Social Indicators Research*, 167(1):475–505, 2023.
- Nicolas Audinet de Pieuchon, Adel Daoud, Connor T. Jerzak, Moa Johansson, and Richard Johansson. Benchmarking debiasing methods for llm-based parameter estimates, 2025. URL <https://arxiv.org/abs/2506.09627>.
- Bradley Efron. Tweedie’s formula and selection bias. *Journal of the American Statistical Association*, 106(496):1602–1614, 2011.
- Bradley Efron. *Large-scale inference: empirical Bayes methods for estimation, testing, and prediction*, volume 1. Cambridge University Press, 2012.

- Naoki Egami, Musashi Hinck, Brandon Stewart, and Hanying Wei. Using imperfect surrogates for downstream inference: Design-based supervised learning for social science applications of large language models. In A. Oh, T. Naumann, A. Globerson, K. Saenko, M. Hardt, and S. Levine, editors, *Advances in Neural Information Processing Systems*, volume 36, pages 68589–68601. Curran Associates, Inc., 2023. URL https://proceedings.neurips.cc/paper_files/paper/2023/file/d862f7f5445255090de13b825b880d59-Paper-Conference.pdf.
- Justin Grimmer, Margaret E Roberts, and Brandon M Stewart. *Text as data: A new framework for machine learning and the social sciences*. Princeton University Press, 2022.
- Neal Jean, Marshall Burke, Michael Xie, W Matthew Davis, David B Lobell, and Stefano Ermon. Combining Satellite Imagery and Machine Learning to Predict Poverty. *Science*, 353(6301):790–794, 2016.
- Connor T Jerzak, Fredrik Johansson, and Adel Daoud. Integrating earth observation data into causal inference: challenges and opportunities. *arXiv preprint arXiv:2301.12985*, 2023a.
- Connor Thomas Jerzak, Fredrik Daniel Johansson, and Adel Daoud. Image-based treatment effect heterogeneity. In *Conference on Causal Learning and Reasoning*, pages 531–552. PMLR, 2023b.
- Mohammad Kakooei, James Bailie, Albin Söderberg, Albin Becevic, and Adel Daoud. Mapping africa settlements: High resolution urban and rural map by deep learning and satellite imagery. *arXiv preprint arXiv:2411.02935*, 2024.
- Shiho Kino, Yu-Tien Hsu, Koichiro Shiba, Yung-Shin Chien, Carol Mita, Ichiro Kawachi, and Adel Daoud. A scoping review on the use of machine learning in research on social determinants of health: Trends and research prospects. *SSM-population Health*, 15:100836, 2021.
- Kerri Lu, Stephen Bates, and Sherrie Wang. Quantifying Uncertainty in Area and Regression Coefficient Estimation from Remote Sensing Maps. *arXiv preprint arXiv:2407.13659*, 2024.
- Ammar Malik, Bradley Parks, Brooke Russell, Joyce Lin, Katherine Walsh, Kyra Solomon, Sheng Zhang, T Elston, and Seth Goodman. Banking on the belt and road: Insights from a new global dataset of 13,427 chinese development projects. *Williamsburg, VA: AidData at William & Mary*, pages 23–36, 2021.
- Pontus Olofsson, Giles M Foody, Stephen V Stehman, and Curtis E Woodcock. Making Better Use of Accuracy Data in Land Change Studies: Estimating Accuracy and Area and Quantifying Uncertainty Using Stratified Estimation. *Remote sensing of environment*, 129:122–131, 2013.
- Markus B Pettersson, Mohammad Kakooei, Julia Ortheden, Fredrik D Johansson, and Adel Daoud. Time series of satellite imagery improve deep learning estimates of neighborhood-level poverty in africa. In *IJCAI*, pages 6165–6173, 2023.
- Nathan Ratledge, Gabe Cadamuro, Brandon de la Cuesta, Matthieu Stigler, and Marshall Burke. Using Machine Learning to Assess the Livelihood Impact of Electricity Access. *Nature*, 611(7936): 491–495, November 2022. ISSN 1476-4687. doi: 10.1038/s41586-022-05322-8. URL <https://www.nature.com/articles/s41586-022-05322-8>. Number: 7936 Publisher: Nature Publishing Group.
- Kazuki Sakamoto, Connor T. Jerzak, and Adel Daoud. A scoping review of earth observation and machine learning for causal inference: Implications for the geography of poverty. In Ola Hall and Ibrahim Wahab, editors, *Geography of Poverty*. 2025.

Di Shu and Grace Y Yi. Causal Inference with Measurement Error in Outcomes: Bias Analysis and Estimation Methods. *Statistical methods in medical research*, 28(7):2049–2068, 2019.

Adam J. Stewart, Nils Lehmann, Isaac A. Corley, Yi Wang, Yi-Chia Chang, Nassim Ait Ali Braham, Shradha Sehgal, Caleb Robinson, and Arindam Banerjee. Ssl4eo-1: Datasets and foundation models for landsat imagery, 2023. URL <https://arxiv.org/abs/2306.09424>.

Yuan-Sen Ting. Why machine learning models systematically underestimate extreme values. *arXiv preprint arXiv:2412.05806*, 2024a.

Yuan-Sen Ting. Why machine learning models systematically underestimate extreme values, 2024b. URL <https://arxiv.org/abs/2412.05806>.

Fucheng Warren Zhu, Connor Thomas Jerzak, and Adel Daoud. Optimizing multi-scale representations to detect effect heterogeneity using earth observation and computer vision: Applications to two anti-poverty rcts. In Biwei Huang and Mathias Drton, editors, *Proceedings of the Fourth Conference on Causal Learning and Reasoning*, volume 275 of *Proceedings of Machine Learning Research*, pages 894–919. PMLR, 07–09 May 2025. URL <https://proceedings.mlr.press/v275/zhu25a.html>.

6 Appendix I. Deriving Implications of Tweedie’s Formula for Causal Debiasing

6.1 Proof of Equation 2

We derive Tweedie’s formula for the posterior mean in the context of the model $\hat{Y}_i = W_i + \varepsilon_i$, where $W_i = kY_i$, $\varepsilon_i \sim \mathcal{N}(0, \sigma^2)$ independent of W_i , and W_i has an arbitrary prior distribution with density $p_W(w)$. The formula holds generally under Gaussian noise and does not require specifying p_W .

Let $p(\hat{y} | w)$ denote the conditional density of \hat{Y}_i given $W_i = w$:

$$p(\hat{y} | w) = \frac{1}{\sqrt{2\pi\sigma^2}} \exp\left(-\frac{(\hat{y} - w)^2}{2\sigma^2}\right).$$

The marginal density of \hat{Y}_i is

$$p_{\hat{Y}}(\hat{y}) = \int_{-\infty}^{\infty} p(\hat{y} | w) p_W(w) dw.$$

The posterior density of W_i given $\hat{Y}_i = \hat{y}$ is

$$p(w | \hat{y}) = \frac{p(\hat{y} | w) p_W(w)}{p_{\hat{Y}}(\hat{y})}.$$

The posterior mean is

$$\mathbb{E}[W_i | \hat{Y}_i = \hat{y}] = \int_{-\infty}^{\infty} w p(w | \hat{y}) dw.$$

To relate this to the derivative of the log-marginal density, start with

$$\log p_{\hat{Y}}(\hat{y}) = \log \left(\int_{-\infty}^{\infty} p(\hat{y} | w) p_W(w) dw \right).$$

Differentiate both sides with respect to \hat{y} , noting that taking the derivative of the logarithm turns the integral of the conditional densities into the integral of their derivatives divided by the overall marginal density:

$$\partial_{\hat{y}} \log p_{\hat{Y}}(\hat{y}) = \frac{1}{p_{\hat{Y}}(\hat{y})} \int_{-\infty}^{\infty} (\partial_{\hat{y}} p(\hat{y} | w)) p_W(w) dw. \quad (5)$$

Now compute $\partial_{\hat{y}} p(\hat{y} | w)$. Since (using the definition of the Gaussian density):

$$\log p(\hat{y} | w) = -\log(\sqrt{2\pi\sigma^2}) - \frac{(\hat{y} - w)^2}{2\sigma^2},$$

we have

$$\partial_{\hat{y}} \log p(\hat{y} | w) = -\frac{1}{2\sigma^2} \cdot 2(\hat{y} - w) = \frac{w - \hat{y}}{\sigma^2}. \quad (6)$$

This is the score function for the Gaussian density, obtained by differentiating the log-likelihood with respect to the observation \hat{y} while treating w as the location parameter.

Because $p(\hat{y} | w) = \exp(\log p(\hat{y} | w))$ and by the chain rule,

$$\partial_{\hat{y}} p(\hat{y} | w) = p(\hat{y} | w) \cdot \frac{w - \hat{y}}{\sigma^2}. \quad (7)$$

Substitute (7) into (5):

$$\begin{aligned} \partial_{\hat{y}} \log p_{\hat{Y}}(\hat{y}) &= \frac{1}{p_{\hat{Y}}(\hat{y})} \int_{-\infty}^{\infty} p(\hat{y} | w) \cdot \frac{w - \hat{y}}{\sigma^2} p_W(w) dw \\ &= \frac{1}{\sigma^2} \int_{-\infty}^{\infty} (w - \hat{y}) p(w | \hat{y}) dw. \end{aligned}$$

The integral is

$$\int_{-\infty}^{\infty} (w - \hat{y}) p(w | \hat{y}) dw = \mathbb{E}[W_i | \hat{Y}_i = \hat{y}] - \hat{y},$$

This holds because, by linearity of expectation, the posterior expectation of $W_i - \hat{y}$ given $\hat{Y}_i = \hat{y}$ equals the posterior expectation of W_i minus \hat{y} , since \hat{y} is a fixed constant under the conditioning.

Therefore,

$$\partial_{\hat{y}} \log p_{\hat{Y}}(\hat{y}) = \frac{\mathbb{E}[W_i | \hat{Y}_i = \hat{y}] - \hat{y}}{\sigma^2}.$$

Solving for the posterior mean yields

$$\mathbb{E}[W_i | \hat{Y}_i = \hat{y}] = \hat{y} + \sigma^2 \partial_{\hat{y}} \log p_{\hat{Y}}(\hat{y}).$$

This completes the proof. The conditional version given treatment $A_i = a$ follows analogously by replacing marginals with conditionals on $A_i = a$, using independence of ε_i and A_i .

6.2 Proof of Proposition 2.3 (Unbiasedness)

We prove the result in two parts: first, that $\mathbb{E}[\tilde{Y}_i | \hat{Y}_i, A_i] = \mathbb{E}[Y_i | \hat{Y}_i, A_i]$ under model (1); second, that $\mathbb{E}[\tilde{Y}_i] = \mathbb{E}[Y_i]$ follows by iterated expectations.

Part 1: Conditional Unbiasedness. Fix $A_i = a \in \{0, 1\}$. All expectations and densities below can be implicitly conditional on $A_i = a$, but we suppress this notation for brevity. Recall the definition: $W_i := kY_i$. Then, under (1), $\hat{Y}_i = W_i + \varepsilon_i$ where $\varepsilon_i \sim \mathcal{N}(0, \sigma^2)$ is independent of W_i (and hence of Y_i).

From the derivation in the proof of Equation 2, the Tweedie formula gives:

$$\mathbb{E}[W_i \mid \hat{Y}_i = \hat{y}] = \hat{y} + \sigma^2 \partial_{\hat{y}} \log p_{\hat{Y}}(\hat{y}).$$

Since $Y_i = W_i/k$,

$$\begin{aligned} \mathbb{E}[Y_i \mid \hat{Y}_i = \hat{y}, A_i = a] &= \frac{1}{k} \mathbb{E}[W_i \mid \hat{Y}_i = \hat{y}, A_i = a] \\ &= \frac{\hat{y} + \sigma^2 \partial_{\hat{y}} \log p_{\hat{Y}|A_i=a}(\hat{y})}{k}. \end{aligned}$$

By definition (4), the Tweedie-adjusted outcome satisfies $\tilde{Y}_i = \mathbb{E}[Y_i \mid \hat{Y}_i, A_i]$. Since \tilde{Y}_i is a deterministic function of (\hat{Y}_i, A_i) from Eq. 4,

$$\mathbb{E}[\tilde{Y}_i \mid \hat{Y}_i, A_i] = \tilde{Y}_i = \mathbb{E}[Y_i \mid \hat{Y}_i, A_i].$$

Part 2: Unconditional Unbiasedness. Unconditional unbiasedness holds by iterated expectations:

$$\mathbb{E}[\tilde{Y}_i] = \mathbb{E} \left[\mathbb{E}[\tilde{Y}_i \mid \hat{Y}_i, A_i] \right] = \mathbb{E} \left[\mathbb{E}[Y_i \mid \hat{Y}_i, A_i] \right] = \mathbb{E}[Y_i].$$

6.3 Proof of Proposition 2.4

We proceed in three steps. Throughout, the probability space encompasses: (i) the *super-population* draw of potential outcomes $\{Y_i(0), Y_i(1)\}_{i=1}^N$; (ii) the independent, additive noise variables $\{\varepsilon_i\}_{i=1}^N$ in (1); and (iii) the random treatment assignment $\{A_i\}_{i=1}^N$, taken to be a completely randomized design that fixes the sample sizes $n_1 = \sum_i A_i$ and $n_0 = \sum_i (1 - A_i)$.

Step 1: Tweedie adjustment is unbiased *within treatment arms*. By definition of \tilde{Y}_i in (4), for every unit i and any realized value \hat{y} of \hat{Y}_i ,

$$\begin{aligned} \mathbb{E}[\tilde{Y}_i \mid \hat{Y}_i = \hat{y}, A_i = a] &= \mathbb{E} \left[\frac{\hat{y} + \sigma^2 \partial_{\hat{y}} \log p_{\hat{Y}|A}(\hat{y} \mid a)}{k} \mid \hat{Y}_i = \hat{y}, A_i = a \right] \\ &= \mathbb{E}[Y_i \mid \hat{Y}_i = \hat{y}, A_i = a], \end{aligned}$$

where the equality is the scaled Tweedie identity (3). Taking expectations over \hat{Y}_i (and using independence of ε_i and A_i),

$$\mathbb{E}[\tilde{Y}_i \mid A_i = a] = \mathbb{E}[Y_i \mid A_i = a]. \quad (8)$$

Step 2: Sample means inherit the same expectation. Fix the realized assignment vector $\mathbf{A} = (A_1, \dots, A_N)$. Because the n_a units with $A_i = a$ form a simple random sample of size n_a from the finite population (complete randomization),

$$\mathbb{E} \left[\frac{1}{n_a} \sum_{i:A_i=a} \tilde{Y}_i \mid \mathbf{A} \right] = \mathbb{E}[\tilde{Y}_i \mid A_i = a], \quad a \in \{0, 1\}.$$

The equality is a consequence of linearity of expectation and the exchangeability of units under random sampling. Specifically, since randomization ensures all units are identically distributed conditional on assignment, the average over the assigned subgroup unbiasedly estimates the conditional expectation over all units. Taking unconditional expectations and invoking (8),

$$\begin{aligned} \mathbb{E}\left[\hat{\mathbb{E}}[\tilde{Y}_i \mid A_i = a]\right] &= \mathbb{E}[\tilde{Y}_i \mid A_i = a] \\ &= \mathbb{E}[Y_i \mid A_i = a], \quad a \in \{0, 1\}. \end{aligned} \tag{9}$$

Step 3: Difference-in-means is asymptotically unbiased for τ . By definition, $\hat{\tau}^T = \hat{\mathbb{E}}[\tilde{Y}_i \mid A_i = 1] - \hat{\mathbb{E}}[\tilde{Y}_i \mid A_i = 0]$. Taking expectations and applying (9),

$$\mathbb{E}[\hat{\tau}^T] = \mathbb{E}[Y_i \mid A_i = 1] - \mathbb{E}[Y_i \mid A_i = 0].$$

Because treatment is randomly assigned, $A_i \perp (Y_i(0), Y_i(1))$, so $\mathbb{E}[Y_i \mid A_i = a] = \mathbb{E}[Y_i(a)]$. Hence

$$\mathbb{E}[\hat{\tau}^T] = \mathbb{E}[Y_i(1)] - \mathbb{E}[Y_i(0)] = \tau,$$

establishing that the Tweedie-corrected difference-in-means estimator is unbiased for the average treatment effect τ when the nuisance parameters (k , σ^2 , and the conditional densities) are known; extensions to asymptotically unbiasedness when they must be estimated are immediate by invoking Slutsky's theorem under regularity conditions..

An empirical analysis using the DHS dataset is presented in Figure A.I.1.

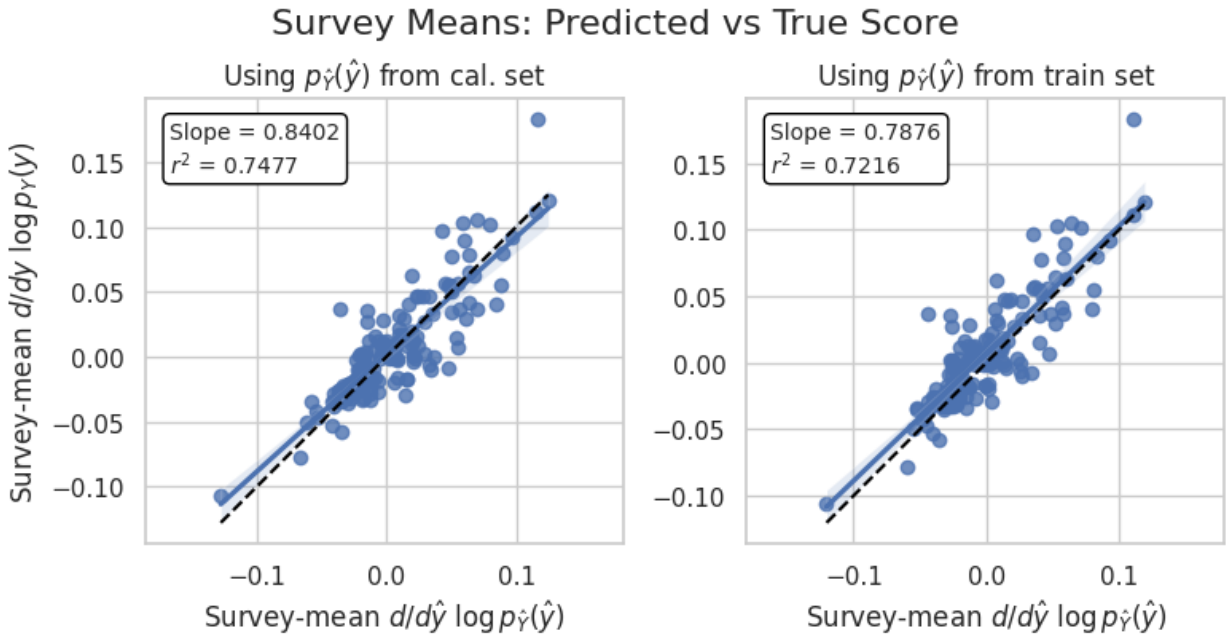


Figure A.I.1: Correlation between the score functions $\frac{d}{dy} \log p_Y(y)$ and $\frac{d}{d\hat{y}} \log p_{\hat{Y}}(\hat{y})$. The plot displays the mean true score (derived from $p_Y(y)$) versus the mean predicted score (derived from $p_{\hat{Y}}(\hat{y})$) for each survey. Score functions estimated from both the held-out calibration set and the training set demonstrate strong correlation with the true score, suggesting that it's feasible to swap the score functions.

7 Appendix II. Model Details

The backbone of each model was a ResNet-50, pre-trained via unsupervised contrastive learning (MOCO) on the SSL4EO-L dataset, as distributed in the TorchGeo library Stewart et al. [2023]. The images were rescaled following the same procedure as in the SSL4EO-L paper, with added data augmentation in the form of random horizontal and vertical flips. A final dense layer was appended to the ResNet to enable the regression task.

Training proceeded for up to 33 epochs. During the first three epochs, we froze all pretrained weights and trained only the newly added final layer. Thereafter, we unfroze the entire network and performed end-to-end fine-tuning with early stopping on the validation set (patience = 5 epochs). Optimization used AdamW with weight decay (ℓ_2 regularization coefficient = 1×10^{-4}), batch size 128 and a cosine learning-rate schedule with warm restarts; analyses use PyTorch 2.6.

The only hyperparameter tuning that was performed was to find the value λ_b used by the Ratledge loss. This was achieved using a grid search, the results of which are presented in Figure A.II.1.

The variables \hat{k} and \hat{m} for the LCC correction were calculated on the fold’s calibration set, while the values for Tweedie’s correction, σ , and the score function were estimated with the training data. For the score function, a Gaussian KDE was fitted using Scott’s rule for determining the bandwidth.

Overall, training models for the five cross-validation folds, comprising one standard MSE-based model and eight Ratledge-loss variants, required approximately nine hours of wall-clock time on a single NVIDIA A100 GPU.

8 Appendix III. Additional Empirical Results

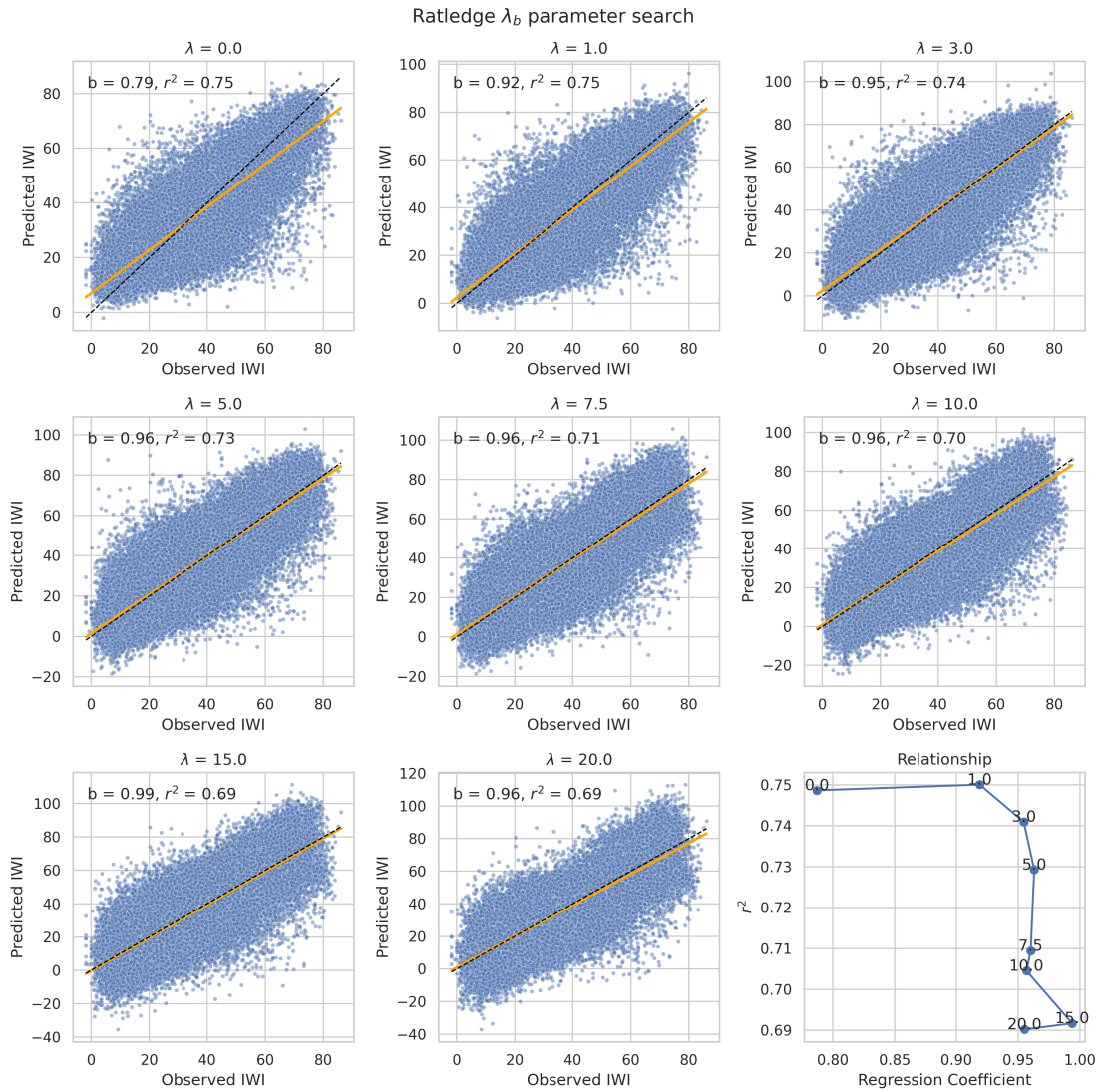


Figure A.II.1: Results of the hyperparameter tuning for finding the best suited λ_b for the Ratledge loss. Based of these results, we opted to use $\lambda_b = 15$ as it had the least shrinkage bias ($b \approx 1$).

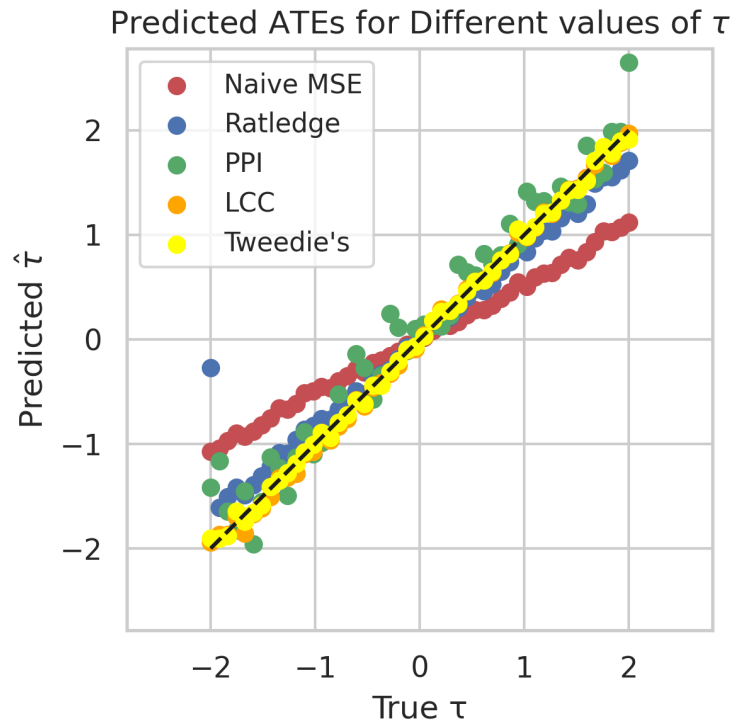


Figure A.III.1: LEFT. Comparison of debiasing methods in a simulated setup varying true ATEs. RIGHT. Simulation performance metrics. F -statistics and p -values are the statistical tests for evaluating the null hypothesis that the slope value is 1. Failure to reject indicates that the slope estimate intervals contain the true ATE.

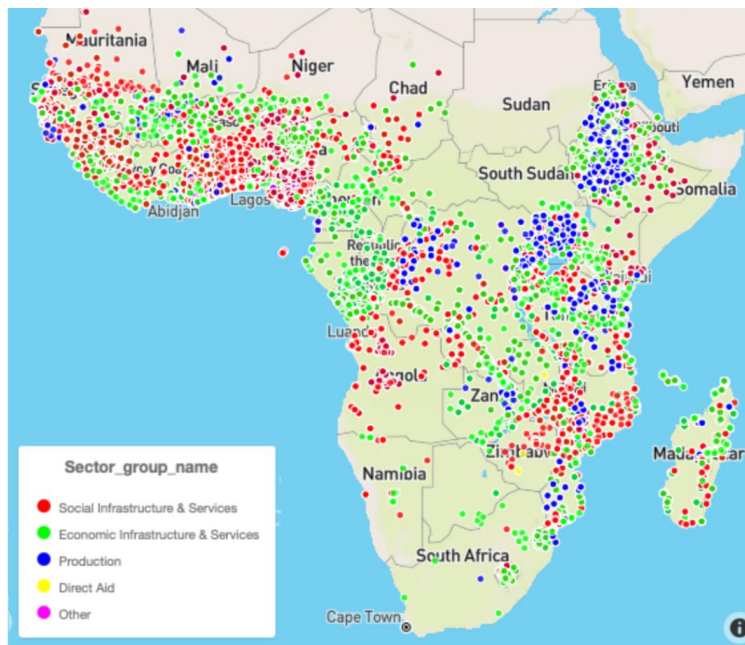


Figure A.III.2: Treatment sites.

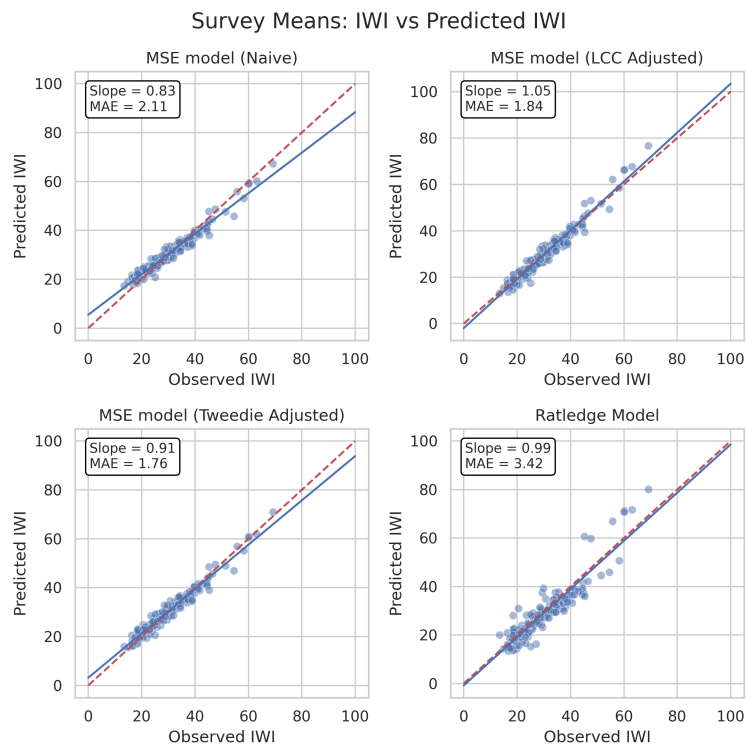


Figure A.III.3: Scatterplot of the observed versus predicted mean IWI for each survey in the test set. The standard MSE-trained model produces biased estimates, overestimating wealth in poorer countries and underestimating it in richer ones. Applying Tweedie’s or LCC adjustments significantly mitigates this shrinkage bias. Training a model with Ratledge loss also mitigates the shrinkage bias, but has a relatively high error in terms of MAE.

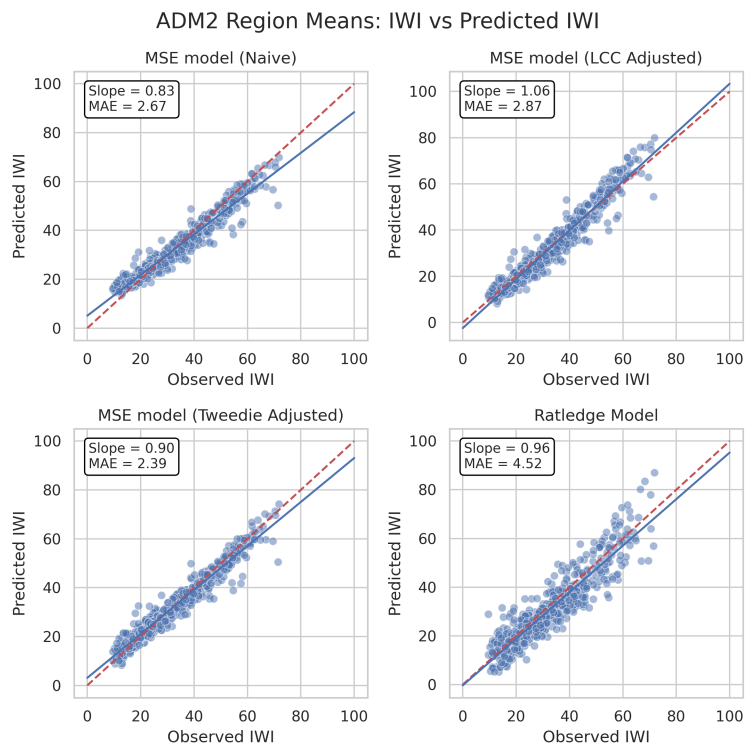


Figure A.III.4: Scatterplot of the observed versus predicted mean IWI for each Admin 2 region in the test set, similar to A.III.3. The standard MSE-trained model produces biased estimates, overestimating wealth in poorer countries and underestimating it in richer ones. Applying Tweedie's or LCC adjustments significantly mitigates this shrinkage bias. Training a model with Ratledge loss also mitigates the shrinkage bias, but has a relatively high error in terms of MAE.

ADM2 Region Means: IWI vs Predicted IWI (Min. 100 samples)

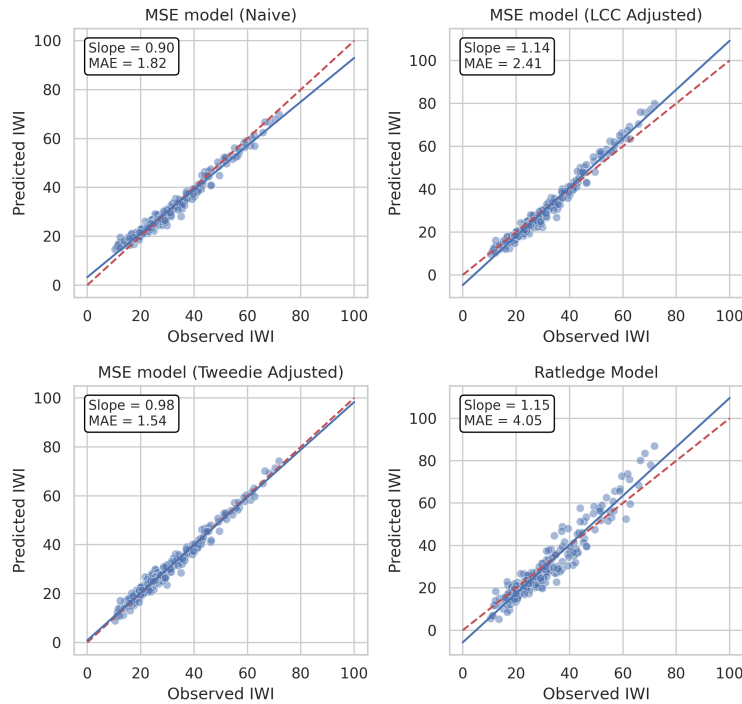


Figure A.III.5: Same as for A.III.4, but only including Admin 2 regions with more than 100 surveyed clusters. The Tweedie adjusted model is now practically unbiased (in regards to shrinkage), suggesting that the correction has larger issues with smaller samples.

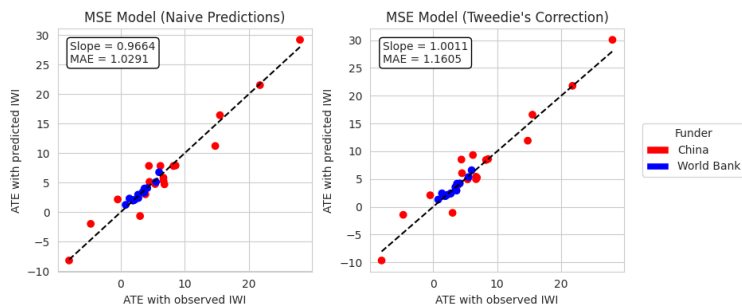


Figure A.III.6: Comparison of predicted treatment effects for aid interventions funded by China versus the World Bank, highlighting differences in estimated impacts across sectors after applying debiasing corrections.

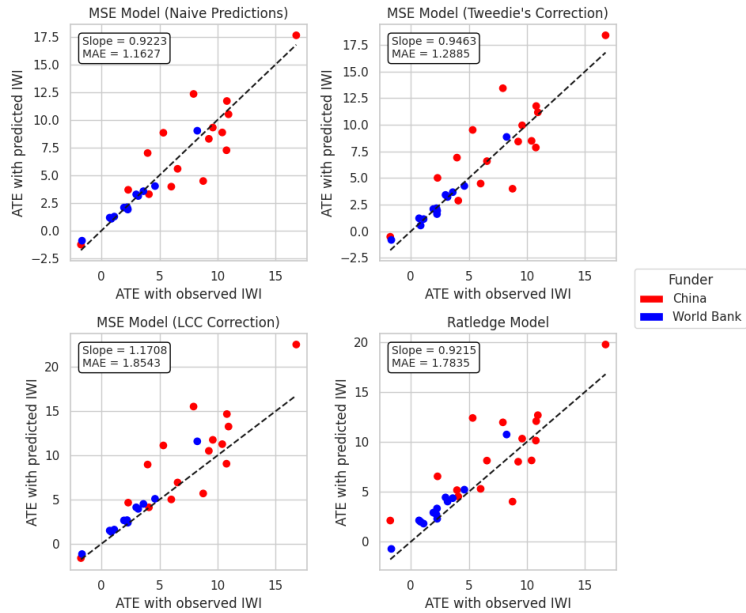


Figure A.III.7: Scatter plots comparing ATE estimated using predicted IWI versus observed IWI for aid interventions funded by China (red points) and the World Bank (blue points). Each panel evaluates a different debiasing approach applied to predictions from an MSE-trained model: (top-left) naive (uncorrected) predictions, (top-right) Tweedie’s correction, (bottom-left) LCC, and (bottom-right) Ratledge model. Dashed black lines represent fitted linear regressions, with slopes and MAE provided; a slope close to 1 indicates reduced attenuation bias toward zero.

Downstream ATE Predictions

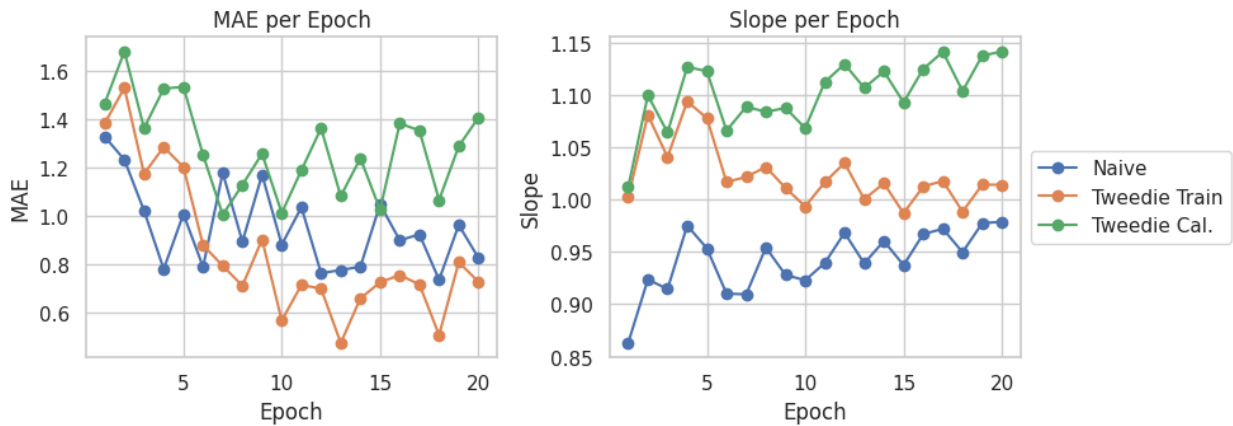


Figure A.III.8: Performance on a downstream causal inference task as a function of upstream model training epochs. Early training (e.g., after one epoch) yields poor model accuracy (high MAE) but minimal overfitting, allowing Tweedie’s correction to produce unbiased estimates using variance from either the calibration set ($\sigma_{\text{Cal.}}$) or training set (σ_{Train}). As epochs increase, model accuracy improves, but growing overfitting causes over-correction when using $\sigma_{\text{Cal.}}$, increasing bias, while σ_{Train} maintains near-unbiased results.

Table A.III.1: Characterization of Debiasing Methods for Causal Inference Using ML Predictions

Method	Data Needs	Training Adjustments	Other Assumptions
(i) <i>PPI</i> [Angelopoulos et al., 2023]	Fresh ground-truth labeled data at the downstream causal inference stage (new treatment-predictor-outcome tuples).	None; treats model as black-box and applies rectifier term.	Predictive model is fixed (not retrained); valid statistical coverage in large samples; independence assumptions for inference.
(ii) <i>Ratledge et al.</i> [2022]	None additional; uses existing upstream training data.	Yes; modifies loss function to include quintile-specific bias penalty ($\mathcal{L} = \text{MSE} + \lambda_r L_2 + \lambda_b \hat{E}_b$). Requires retraining.	Bias reducible by penalizing group-level discrepancies; assumes quintile-based error structure.
(iii) <i>DSL</i> [Egami et al., 2023]	Gold-standard labeled data on a subset of units (no new data collection); known or estimated sampling probabilities depending on surrogates and covariates.	None; post-hoc construction of bias-corrected pseudo-outcomes via cross-fitting and doubly-robust estimation.	Known sampling design with probabilities bounded away from zero; double robustness (consistent if either outcome model or sampling model is correctly specified).
(iv) <i>LCC</i> (this work)	Held-out calibration data from upstream training phase (no new data collection).	None; post-hoc linear transformation on predictions.	Linear shrinkage model ($\hat{Y}_i = kY_i + m$ with $0 < k \leq 1$).
(v) <i>Tweedie's correction</i> (this work)	Held-out data from upstream for estimating σ^2 and score function (no new data collection).	None; post-hoc adjustment using empirical Bayes and density scores.	Gaussian homoskedastic noise ($\hat{Y}_i = Y_i - \varepsilon_i$, $\varepsilon_i \sim \mathcal{N}(0, \sigma^2)$) independent of Y_i ; $\mathbb{E}[\varepsilon_i A_i] = 0$.

Funder	Sector Code	AD Sector Name	Observed ATE (IWI)	Naive Predicted ATE (IWI)	Tweedie's ATE (IWI)	Num. Treated Clusters	Num. Control Clusters
CH	110	Education	13.02	13.01	13.36	1549	22381
WB	110	Education	7.33	7.77	7.79	6285	24262
WB	120	Health	3.75	4.05	4.11	6965	24411
CH	120	Health	19.71	19.38	19.86	3333	32198
CH	130	Population Policies/Programmes	11.30	9.06	9.42	60	335
WB	140	Water Supply and Sanitation	8.04	7.77	7.86	10470	27888
CH	140	Water Supply and Sanitation	19.08	17.32	17.69	676	7883
CH	150	Government and Civil Society	21.55	20.88	21.31	1860	22983
WB	150	Government and Civil Society	2.18	2.47	2.33	16027	25739
WB	160	Other Social Infrastructure and Services	5.48	5.28	5.65	9178	25226
CH	160	Other Social Infrastructure and Services	20.15	19.40	19.75	843	13557
CH	210	Transport and Storage	20.16	18.79	19.19	1509	14122
WB	210	Transport and Storage	3.81	3.99	3.66	12550	28163
WB	220	Communications	0.50	1.60	0.84	1537	11327
CH	220	Communications	12.42	12.22	12.36	997	6371
WB	230	Energy Generation and Supply	7.16	7.23	7.35	6683	25702
CH	230	Energy Generation and Supply	13.00	13.07	12.97	357	7958
WB	240	Banking and Financial Services	8.14	7.63	8.30	2363	14997
WB	310	Agriculture, Forestry and Fishing	3.21	3.09	3.10	8907	25187
CH	310	Agriculture, Forestry and Fishing	4.49	4.35	3.78	949	10400
WB	320	Industry, Mining, Construction	2.80	2.86	2.95	5183	23180
CH	320	Industry, Mining, Construction	21.31	23.75	24.21	74	2041
WB	330	Trade and Tourism	2.63	4.07	3.46	840	7852
CH	330	Trade and Tourism	19.10	20.12	20.48	52	487
WB	410	General Environment Protection	13.06	14.03	13.94	1284	11273
CH	420	Women in Development	18.95	18.53	18.89	81	3238
CH	430	Other Multisector	26.74	25.06	25.93	225	3755
CH	520	Developmental Food Aid/Food Security	18.20	17.89	18.92	170	2163
CH	700	Emergency Response	11.24	10.54	10.74	258	5090

Table A.III.2: Overview: Aid sector effect estimates.

Country	# Clusters	—IWI—		Survey Years	Urban %
		Mean	SD		
Angola	969	32.68	24.06	06-07, 11, 15-16	50.2
Benin	1567	28.82	13.31	96, 01, 11-12, 17-18	43.7
Burkina Faso	2232	26.52	12.18	93, 98-99, 03, 10, 14, 17-18, 21	32.8
Burundi	1128	19.01	10.81	10, 12, 16-17	19.2
C.A.F.	90	13.52	4.57	94-95	30.0
Cameroon	1920	35.95	17.23	91, 04, 11, 18, 22	53.6
Chad	624	16.25	10.74	14-15	26.1
Comoros	242	38.37	12.38	12	43.8
Côte d'Ivoire	1113	37.84	14.19	94, 98-99, 11-12, 21	52.3
D.R.C.	783	18.34	14.04	07, 13-14	35.9
Egypt	7637	59.39	11.79	92, 95, 00, 03, 05, 08, 14	48.2
Eswatini	270	38.00	13.50	06-07	40.4
Ethiopia	2532	17.78	15.29	00, 05, 11, 16, 19	29.2
Gabon	719	43.10	16.50	12, 19-21	59.0
Gambia	280	51.17	14.75	19-20	61.8
Ghana	2456	39.11	15.77	93, 98, 03, 08, 14, 16, 19, 22	45.8
Guinea	1442	30.04	15.60	99, 05, 12, 18, 21	35.9
Kenya	4605	30.41	14.85	03, 08-09, 14, 15, 20, 22	38.9
Lesotho	1162	26.72	12.23	04, 09, 14	27.1
Liberia	1534	21.45	12.64	07, 09, 11, 13, 16, 19-20, 22	40.7
Madagascar	2393	21.25	12.86	97, 08-09, 11, 13, 16, 21	25.8
Malawi	3184	19.68	9.31	00, 04, 10, 12, 14, 15-16, 17	20.5
Mali	2182	26.90	13.48	95-96, 01, 06, 12-13, 15, 18, 21	32.5
Mauritania	1198	38.18	18.67	19-21	47.2
Morocco	476	54.56	17.11	03-04	56.7
Mozambique	1406	26.41	16.91	09, 11, 15, 18	42.7
Namibia	1301	37.29	21.03	00, 06-07, 13	44.7
Niger	899	21.52	15.04	92, 98, 12, 21	36.2
Nigeria	4641	36.78	18.08	03, 08, 10, 13, 15, 18, 21	38.7
Rwanda	2185	22.12	9.34	05, 07-08, 10, 14-15, 19-20	21.6
Senegal	3387	37.48	16.81	92-93, 97, 05, 08-09, 10-11, 12-19, 20-21	41.1
Sierra Leone	1678	24.21	13.97	08, 13, 16, 19	36.3
South Africa	746	58.23	14.43	16	62.2
Tanzania	3626	24.48	13.97	99, 03-04, 07-08, 10, 11-12, 15-16, 17, 22	27.7
Togo	621	30.83	15.18	98, 13-14, 17	37.8
Uganda	2417	24.89	13.52	00-01, 06, 09, 11, 14-15, 16, 18-19	27.2
Zambia	1573	26.73	17.96	07, 13-14, 18	39.2
Zimbabwe	1401	32.83	17.83	99, 05-06, 10-11, 15	38.1
Total	68619	32.59	19.11	-	37.8

Table A.III.3: Overview of data: DHS surveys on health and living conditions.

9 Appendix IV. Simulation Design

In this DAG, C_i is a confounder that influences both the treatment assignment A_{is} and the outcome Y_i . Our simulation samples it from a standard Normal distribution, $C_i \sim \mathcal{N}(0, 1)$. The treatment A_{is} (we suppress the index s henceforth) is assigned probabilistically based on C_i using a sigmoid function:

$$A_i \sim \text{Bernoulli} \left(\frac{1}{1 + \exp(-C_i)} \right) \quad (10)$$

The outcome, Y_i , is then generated as:

$$Y_i \sim \mathcal{N}(\tau A_i + C_i, \sigma_Y)$$

This formulation implies that higher values of C_i both increase the likelihood of treatment and the expected outcome.

To emulate a real-world scenario in which outcomes are not directly observed but inferred from complex data (e.g., satellite imagery), we construct a latent representation $\mathbf{X}_i = g(Y_i)$. Here, g is a randomly initialized three-layer neural network with ReLU activations. The network takes scalar Y_i as input, processes it through hidden layers of dimension 50, and outputs a 100-dimensional embedding \mathbf{X}_i .

A separate model, f , is then trained to predict the outcome, Y , from the embedding, \mathbf{X}_i . The resulting predictions $\hat{Y}_i = f(\mathbf{X}_i)$ are used to estimate the treatment effect τ via Inverse Probability of Treatment Weighting (IPTW), with the treatment probability given as in Eq. 10.

To compare the different debiasing approaches, IPTW estimates were computed for various predicted values.

We run an experiment to simulate a full prediction-to-causal-inference pipeline using synthetic data. For a given value of τ , we generate a training population according to the predefined causal DAG. To construct embeddings \mathbf{X}_i , we initialize a neural network g with random, frozen weights. This network maps the scalar outcome Y_i to a 100-dimensional embedding: $\mathbf{X}_i = g(Y_i)$. This setup induces a non-linear and noisy relationship between Y_i and \mathbf{X}_i , mimicking real-world scenarios where predictive features encode partial and indirect information about outcomes.

We then train a separate neural network f to predict Y_i from \mathbf{X}_i using the standard mean squared error loss, producing predicted values $\hat{Y}_i = f(\mathbf{X}_i)$. A test population is generated using the same DAG, parameter settings, and embedding function, g . From this test population, we compute multiple different estimates of the treatment effect, as described below, using the trained model outputs with corrections. To evaluate the robustness of our findings to hyperparameter choice of τ , we repeat this entire process across 51 evenly spaced values of τ in the range $[-2, 2]$. On average, the predictions, \hat{Y}_i , of model f get a mean R^2 value of about 0.5 when used to predict Y_i .

First, we compute the SAMPLE ATE using inverse probability of treatment weighting (IPTW) on the true labels Y . As this is based on finite samples, it provides a noisy, but approximately unbiased, estimate of τ . Next, we compute the PREDICTED ATE using the predicted outcomes \hat{Y}_i instead of Y_i . As expected, this estimate exhibits shrinkage bias, systematically pulling $\hat{\tau}$ toward zero. Finally, we apply the four debiasing methods mentioned above to the predicted outcomes to produce corrected estimates.

10 Appendix V. World Bank and China Empirical Case

For robustness, we repeat this experiment, using urban/rural, country, and survey year as confounders (Figure A.III.6). The results show that this approach breaks the bias in terms of treatment effect. For larger studies, with more than 200 treated points, it also lowers the total error rate. We hypothesize that the reason

the overall error rate does not decrease for small trials is due to the added variance introduced when calculating the Tweedie correction. The correction is a mean of the sample scores, and it decreases with larger sample sizes.